Autonomous control for satellite rendezvous in near-Earth orbits

Vivek Muralidharan
Space Robotics Research Group
University of Luxembourg, Luxembourg
vivek.muralidharan@uni.lu

Carol Martinez
Space Robotics Research Group
University of Luxembourg, Luxembourg
carol.martinezluna@uni.lu

Augustinas Žinys
Blackswan Space
Vilnius, Lithuania
augustinas@blackswan.ltd

Marius Klimavičius
Blackswan Space
Vilnius, Lithuania
marius@blackswan.ltd

Miguel Olivares-Mendez
Space Robotics Research Group
University of Luxembourg, Luxembourg
miguel.olivaresmendez@uni.lu

***Abstract*—CubeSats are being deployed for a number of activities including Earth observation, telecommunications, scientific experiments, and due to their low cost and flexibility, more often than not, they are even being considered for use in On-Orbit Servicing (OOS) and debris removal missions. This investigation focuses on using the CubeSat technology to perform autonomous proximity operations with passive target bodies including satellites or space debris. The nonlinear coupled attitude and orbit dynamics for the chaser and the target bodies are modelled and simulated. A nonlinear optimal controller identifies an appropriate rendezvous path. A vision-based navigation system on the chaser satellite records the pose of the target body. The pose observations with stochastic uncertainties are processed using a Kalman filter, and offer state feedback along the satellite path. Such observations in conjunction with the postulated linear control algorithm anchor the chaser to approach the target by maintaining appropriate relative configuration. The linear controller delivers regular maneuvers to compensate for any deviations from the identified reference path. A close-range rendezvous operation is illustrated in a Mission Design Simulator (MDS) tool.**

***Index Terms*—satellite rendezvous, coupled orbit attitude dynamics, nonlinear optimal control, vision-based navigation, linear control, on-orbit servicing (OOS), Clohessy-Wiltshire model, Kalman filter, proximity operations**

I. Introduction

Proximity operations such as rendezvous and docking/berthing play a crucial role as a sustainable solution for the use of space. Such operations are crucial in carrying out a variety of tasks including On-Orbit Servicing to restore or improve functionality of operational satellites, life extension through refueling, capturing and de-orbiting of defunct satellites and other space debris. Missions with humans on-board have facilitated several rendezvous operations but they are expensive and risky. Moreover, large scale manned missions are not feasible. Alternately, CubeSats are inexpensive and adept for large scale operations.

This investigation focuses on autonomous Guidance, Navigation and Control (GNC) technique for orbital rendezvous. Clohessy-Wiltshire equations of motions describe the nonlinear relative orbital motion between the chaser and the target. The target object is considered under the influence of gravity gradient torque without any attitude control. The chaser satellite, however, consists of active orbit and attitude controls. Each of the target and chaser satellites are considered as rigid body and must maintain a fixed distance from each other during the rendezvous operations. A two-layered control approach is exercised for the proximity operations; firstly, a nonlinear control is employed to identify a baseline approach path, and subsequently, a linear controller overcomes any deviations from this predetermined baseline path. Vision-based navigation system determines the relative configuration between the chaser and the target, and offers feedback to the control algorithm. Finally, the Mission Design Simulator (MDS) software is applied in-the-loop with the GNC algorithm to validate the architecture.

II. Relative Satellite Dynamics

For close proximity operations between a chaser body and a target body, as in a rendezvous scenario, the relative orbital dynamics are suffice to represent the motion of one body with respect to the other. Such dynamics is valid for bodies including controllable objects such as satellites as well as defunct satellites and any debris objects. A significant number of man-made objects in space orbit in nearly circular Low Earth Orbits.[1] Suitably, Clohessy-Wiltshire model (defined in the coordinate system $\underline{R}$ as in Fig. 1) offers simplified equations to represent the relative nonlinear dynamics of a chaser body with respect to a target body in a circular orbit,[2] and have been employed for several rendezvous and formation flying applications.[2–8] The relative dynamics of the chaser body with respect to the target is governed by

$$\ddot{x} = 3\Omega^2 x + 2\Omega\dot{y} + u_1 \tag{1}$$

$$\ddot{y} = -2\Omega\dot{x} + u_2 \tag{2}$$

$$\ddot{z} = -\Omega^2 z + u_3 \tag{3}$$

where, $\bar{\rho} = x\hat{x} + y\hat{y} + z\hat{z}$. Here, $\Omega = \sqrt{\mu/a^3}$ is the orbital angular velocity for the target body in an orbit with radius a, and, μ, is the Standard gravitational parameter for Earth.

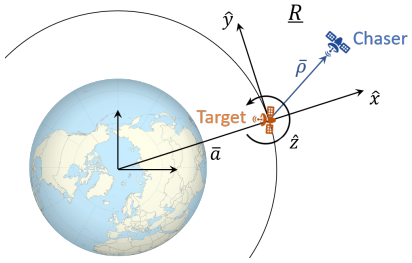

Fig. 1. Rotating coordinate frame, $\underline{R}$, centered at the target to represent the Clohessy-Wiltshire model. Direction $\hat{x}$ points radially away from the Earth, $\hat{y}$ points in the direction of orbit velocity and $\hat{z}$ completes the dextral coordinate system pointing in the direction of the positive angular momentum vector.

The attitude dynamics for the chaser are expressed relative to the target body for simplicity of rendezvous operations. As a consequence, the quantities for angular velocity and orientation quaternions are expressed as

$$ {}^{C}\dot{\omega}_1 = \frac{1}{{}^{C}I_1}\left(T_1 - \left({}^{C}I_3 - {}^{C}I_2\right){}^{C}\omega_2{}^{C}\omega_3\right) \tag{4} $$

$$ {}^{C}\dot{\omega}_2 = \frac{1}{{}^{C}I_2}\left(T_2 - \left({}^{C}I_1 - {}^{C}I_3\right){}^{C}\omega_1{}^{C}\omega_3\right) \tag{5} $$

$$ {}^{C}\dot{\omega}_3 = \frac{1}{{}^{C}I_3}\left(T_3 - \left({}^{C}I_2 - {}^{C}I_1\right){}^{C}\omega_1{}^{C}\omega_2\right) \tag{6} $$

$$ {}^{C}\dot{\epsilon}_1 = \frac{1}{2}\left({}^{C}\omega_1{}^{C}\epsilon_4 - {}^{C}\omega_2{}^{C}\epsilon_3 + {}^{C}\omega_3{}^{C}\epsilon_2\right) \tag{7} $$

$$ {}^{C}\dot{\epsilon}_2 = \frac{1}{2}\left({}^{C}\omega_1{}^{C}\epsilon_3 + {}^{C}\omega_2{}^{C}\epsilon_4 - {}^{C}\omega_3{}^{C}\epsilon_1\right) \tag{8} $$

$$ {}^{C}\dot{\epsilon}_3 = \frac{1}{2}\left(-{}^{C}\omega_1{}^{C}\epsilon_2 + {}^{C}\omega_2{}^{C}\epsilon_1 + {}^{C}\omega_3{}^{C}\epsilon_4\right) \tag{9} $$

$$ {}^{C}\dot{\epsilon}_4 = \frac{1}{2}\left(-{}^{C}\omega_1{}^{C}\epsilon_1 - {}^{C}\omega_2{}^{C}\epsilon_2 - {}^{C}\omega_3{}^{C}\epsilon_3\right) \tag{10} $$

where ${}^{C}\omega \equiv \omega(Chaser \rightarrow Target)$ and ${}^{C}\epsilon_i \equiv \epsilon_i(Chaser \rightarrow Target)$ with a left superscript, C. The dynamics of the target body are expressed relative to the inertial frame. Notations for the angular velocity and orientation quaternions are expressed with a left superscript, T, for example, ${}^{T}\omega \equiv \omega(Target \rightarrow Inertial)$. The target body is modelled such that the gravity torque affects its motion and may potentially deliver a non-cooperative tumbling scenario. The equations for attitude dynamics for the target are governed by

$$ {}^{T}\dot{\omega}_1 = \frac{{}^{T}I_3 - {}^{T}I_2}{{}^{T}I_1}\left(3\mathbb{C}_{12}\mathbb{C}_{13}\Omega^2 - {}^{T}\omega_2{}^{T}\omega_3\right) \tag{11} $$

$$ {}^{T}\dot{\omega}_2 = \frac{{}^{T}I_1 - {}^{T}I_3}{{}^{T}I_2}\left(3\mathbb{C}_{11}\mathbb{C}_{13}\Omega^2 - {}^{T}\omega_1{}^{T}\omega_3\right) \tag{12} $$

$$ {}^{T}\dot{\omega}_3 = \frac{{}^{T}I_2 - {}^{T}I_1}{{}^{T}I_3}\left(3\mathbb{C}_{11}\mathbb{C}_{12}\Omega^2 - {}^{T}\omega_1{}^{T}\omega_2\right) \tag{13} $$

$$ {}^{T}\dot{\epsilon}_1 = \frac{1}{2}\left({}^{T}\omega_1{}^{T}\epsilon_4 - {}^{T}\omega_2{}^{T}\epsilon_3 + {}^{T}\omega_3{}^{T}\epsilon_2\right) \tag{14} $$

$$ {}^{T}\dot{\epsilon}_2 = \frac{1}{2}\left({}^{T}\omega_1{}^{T}\epsilon_3 + {}^{T}\omega_2{}^{T}\epsilon_4 - {}^{T}\omega_3{}^{T}\epsilon_1\right) \tag{15} $$

$$ {}^{T}\dot{\epsilon}_3 = \frac{1}{2}\left(-{}^{T}\omega_1{}^{T}\epsilon_2 + {}^{T}\omega_2{}^{T}\epsilon_1 + {}^{T}\omega_3{}^{T}\epsilon_4\right) \tag{16} $$

$$ {}^{T}\dot{\epsilon}_4 = \frac{1}{2}\left(-{}^{T}\omega_1{}^{T}\epsilon_1 - {}^{T}\omega_2{}^{T}\epsilon_2 - {}^{T}\omega_3{}^{T}\epsilon_3\right) \tag{17} $$

where, $\mathbb{C}$ is the rotation matrix corresponding to the transformation between target body frame and rotating coordinate frame, $\underline{R}$; and $\mathbb{C}_{ij}$ is the element in the i-th row and j-th column. With specific initial conditions for the target body a non-tumbling motion balanced by gravity torque is produced. Each of the chaser and target bodies are considered to be rigid, and therefore, while rendezvous, the chaser satellite must stay at a fixed distance from the target body without colliding. Such a location, labelled as 'approach site,' is defined by

$$ {}^{T}\bar{\varrho}^{B} = d_1\hat{b}_1 + d_2\hat{b}_2 + d_3\hat{b}_3 $$

and is stationary in the target's body fixed frame B defined by unit vectors $\hat{b}_1\hat{b}_2\hat{b}_3$. Here, preceding superscript T in ${}^{T}\bar{\varrho}^{B}$ refers to the target body, while superscript B represents the body frame. The coordinates of the approach site, however, is not fixed in the inertial frame, or the Clohessy-Wiltshire rotating coordinate frame. In case of a tumbling target, the approach site is rather a 3-dimensional path continuous in time, as illustrated in Fig. 2. In this investigation, the approach site is the location of the geometric center of the chaser satellite for rendezvous. With coordinate transformation ($\mathfrak{C} : T \rightarrow I$), the approach site in the inertial frame is represented as

$$ {}^{T}\bar{\varrho}^{I} = [D_1,\ D_2,\ D_3]^{\mathrm{T}} = \mathfrak{C}\ {}^{T}\bar{\varrho}^{B} = \mathfrak{C}\,[d_1,\ d_2,\ d_3]^{\mathrm{T}} $$

however, the Clohessy-Wiltshire rotating frame is the working frame of view and offers direct understanding of the satellite approach within the rendezvous process. The path in the rotating frame is converted from the inertial view as

$$ x_\varrho = D_1 cos(\Omega t) + D_2 sin(\Omega t) \tag{18} $$

$$ y_\varrho = -D_1 sin(\Omega t) + D_2 cos(\Omega t) \tag{19} $$

$$ z_\varrho = D_3 \tag{20} $$

where subscript 'ϱ' refers to the approach site. Within the rendezvous process, the chaser satellite advances towards the approach site.For simplicity, the location of the approach site in the rotating frame is expressed as $\bar{\varrho}^{\underline{R}} = [x_\varrho, y_\varrho, z_\varrho]^{\mathrm{T}}$.

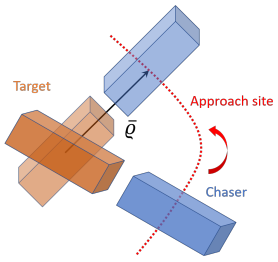

Fig. 2. Approach site, $\bar{\varrho}$, as a 3D location relative to the center of the target.

III. Optimal Trajectory and Attitude Planning

The equations of motion that governs the trajectory and the attitude dynamics for the chaser satellite relative to the target is clearly nonlinear. To initiate an effective rendezvous operation a suitable path that drives the chaser towards the target is desired. Moreover, the relative orientation of the chaser and the target must be consistent alongside. A nonlinear control

algorithm, CasADi, is introduced with the Interior Point Optimization (IPOPT) method to deliver an optimal trajectory and attitude plan adequate for the proximity operations.[9] The controller minimizes the cost function, J, such that

$$J = \int_0^\tau (\bar{\rho} - \bar{\varrho}^{\underline{R}})^{\mathrm{T}} \mathbf{Q}_1 (\bar{\rho} - \bar{\varrho}^{\underline{R}}) + {}^{C}\bar{\omega}^{\mathrm{T}} \mathbf{Q}_2 {}^{C}\bar{\omega} + {}^{C}\bar{\epsilon}^{\mathrm{T}} \mathbf{Q}_3 {}^{C}\bar{\epsilon} + \mathbf{u}^{\mathrm{T}} \mathbf{R} \mathbf{u} \quad dt \tag{21}$$

where the position deviation from the approach site, i.e., $\bar{\rho} - \bar{\varrho}^{\underline{R}}$ is weighted by matrix $\mathbf{Q}_1$, the angular velocity of the chaser relative to the target is weighted by matrix $\mathbf{Q}_2$, the relative orientation between the two satellites by matrix $\mathbf{Q}_3$, and finally, the control inputs $\mathbf{u}$ by weighting matrix $\mathbf{R}$. The control input vector $\mathbf{u}_k$ is defined as,

$$\mathbf{u}_k = [u_1, u_2, u_3, T_1, T_2, T_3]^{\mathrm{T}}$$

includes translational acceleration u_1, u_2 and u_3 along each of x, y and z directions, respectively, as well as the control torques T_1, T_2 and T_3 (also referred as u_4, u_5 and u_6) that the reaction wheels within the chaser satellite are capable to deliver. An additional collision avoidance constraint is introduced such as

$$||\bar{\rho}|| \geq r_{collision}$$

to keep the chaser away from a spherical volume around the target of radius $r_{collision}$. The optimal trajectory and attitude states obtained serve as the baseline or the predicted reference path for rendezvous operations. The optimal path, however, does not account for any uncertainties in state estimation, as a consequence, state estimation and concurrent control algorithm is engaged in-sync throughout the entire process.

IV. Estimation and Linear Control

A. State Estimation

For close-range rendezvous operations, the vision-based sensors on the chaser satellite tracks the pose (position and orientation vectors) of the target satellite, or any target object including debris. For far-range rendezvous operations where the distance between the chaser and the target body is significant, pose measurements may not be reliable, instead range and line-of-sight (LOS) measurements can be recorded. A measurement matrix is computed for every observation that contains partials of observed state, i.e., pose or range and LOS measurements, with respect to the state variables. Prior observations may be discarded in the case of a sequential Kalman filter, thus, offering advantage over a batch least squares filter in terms of computational memory allocation.[10] Consequently, a sequential Kalman filter is selected for this analysis.

1) System Dynamics: Consider the state vector $\mathbf{x}$ such that,

$$\mathbf{x} = [x, y, z, \dot{x}, \dot{y}, \dot{z}, {}^{C}\omega_1, {}^{C}\omega_2, {}^{C}\omega_3, {}^{C}\epsilon_1, {}^{C}\epsilon_2, {}^{C}\epsilon_3, {}^{C}\epsilon_4, {}^{T}\omega_1, {}^{T}\omega_2, {}^{T}\omega_3, {}^{T}\epsilon_1, {}^{T}\epsilon_2, {}^{T}\epsilon_3, {}^{T}\epsilon_4, x_\varrho, y_\varrho, z_\varrho]^{\mathrm{T}}$$

and contains information on the position and the velocity of the chaser relative to the target, orientation of the chaser relative to the target, orientation of the target body relative to the inertial frame, and the location along the approach site at a given instance. The orientation of the target body relative to the Inertial frame as well as the instantaneous location of the approach site evolve independent of the dynamics of the chaser satellite. As a consequence, pose, range and LOS estimation are decoupled from these state elements.

The Kalman filter sequentially updates the covariance with every observed data and thus estimates the states within the stochastic system. A linearized system of state equations about the baseline optimal path for the satellite motion is considered for the Kalman filter to expedite the computational process. The equations are as formulated

$$\delta\mathbf{x}_{j+1} = \mathbf{A}_j \delta\mathbf{x}_j + \mathbf{B}_j \Delta\mathbf{v}_j + \mathbf{w}_j \tag{22}$$

$$\delta\mathbf{y}_{j+1} = \mathbf{H}_j \delta\mathbf{x}_j + \mathbf{e}_j \tag{23}$$

where $\mathbf{H}_j = \frac{\partial \mathbf{y}}{\partial \mathbf{x}}$, while $\mathbf{w}_j$ and $\mathbf{e}_j$ are stochastic white noise with covariance $E[\mathbf{w}_j \mathbf{w}_j^{\mathrm{T}}] = \mathbb{Q}$ and $E[\mathbf{e}_j \mathbf{e}_j^{\mathrm{T}}] = \mathbb{R}$. Control inputs may not be delivered at all the sampling locations, therefore, the value for $\Delta\mathbf{v}_j$ may be zero at time t_j.

2) Filtering: Individual observations may not deliver accurate estimate of the states. Therefore, filtering techniques are used to identify the state variables with reasonable precision. The Kalman filter assumes that the noises, w_j and e_j, are Gaussian. Such an assumption is reasonable and delivers adequate results, as in literature.[11] The resulting equations for state estimation using sequential Kalman filter are

$$\delta\hat{\mathbf{x}}_{j|j} = \delta\hat{\mathbf{x}}_{j|j-1} + \mathbb{K}_j \delta\mathbf{y}_j \tag{24}$$

$$\mathbf{\Sigma}_{j|j} = \mathbf{\Sigma}_{j|j-1} - \mathbb{K}'_j \mathbf{H}_j \mathbf{\Sigma}_{j|j-1} \tag{25}$$

$$\mathbb{K}'_j = \mathbf{\Sigma}_{j,j-1} \mathbf{H}_j^T (\mathbf{H}_j \mathbf{\Sigma}_{j|j-1} \mathbf{H}_j^T + \mathbb{R})^{-1} \tag{26}$$

$$\mathbf{\Sigma}_{j+1|j} = \mathbf{A}_j \mathbf{\Sigma}_{j|j} \mathbf{A}_j^T + \mathbb{Q}_j \tag{27}$$

where $\delta\hat{\mathbf{x}}_{j|j-1}$ is the predicted estimate from the state equations of measurement $j-1$, and $\delta\hat{\mathbf{x}}_{j|j}$ is the new estimate using the filter for measurement j. Kalman gain, $\mathbb{K}$, is dependent on the output measurement, output variance, and state variance. The covariance matrix

$$\mathbf{\Sigma}_{j|j-1} = E[(\delta\mathbf{x}_j - \delta\hat{\mathbf{x}}_{j|j-1})(\delta\mathbf{x}_j - \delta\hat{\mathbf{x}}_{j|j-1})^{\mathrm{T}}] \tag{28}$$

is the *a-priori* covariance based upon $j-1$-th observation while the covariance matrix

$$\mathbf{\Sigma}_{j|j} = E[(\delta\mathbf{x}_j - \delta\hat{\mathbf{x}}_{j|j})(\delta\mathbf{x}_j - \delta\hat{\mathbf{x}}_{j|j})^{\mathrm{T}}] \tag{29}$$

is the *a-posteriori* covariance computed once the j-th observation is available. In the beginning, when no observed data are available, the *a-priori* covariance $\mathbf{\Sigma}_{j|j-1}$ is set to a very large value. With additional observations, the covariance matrix is updated. Pose data are extracted at finite time intervals, and at a significantly faster rate than the delivery of the maneuvers, allowing ample time to record enough observations and to get a reliable estimate.

B. Linear Controller

A nonlinear controller is certainly adept, and superior to a linear controller, at evaluating the coupled nonlinear and time-variant orbit and attitude dynamics of the system; subsequently implemented to identify an efficient path for proximity operations once the initial conditions for the states of the chaser and the target are determined. The computational time required for a nonlinear controller is substantially higher than that of a linear controller. Controller must compute and deliver outputs at a pace faster than the actual flight time, so that the satellite is able to operate in synchronization with any on-board satellite software, mission simulation software, or a vision-based navigation system. As a consequence, despite the advantages offered by a nonlinear controller, it is not adopted for the routine process, instead, a rapid linear controller is blended with the nonlinear optimal control to deliver maneuvers to compensate any deviations from the predetermined reference path.

A two-layered control approach is employed to combine the benefits offered by the nonlinear and the linear controller. First and foremost, the nonlinear controller identifies an ideal sequence of control outputs and state history for the rendezvous operations, and serves as the baseline approach path. The first control output computed by the nonlinear controller is delivered. Subsequent maneuvers are determined by the linear controller that overcome any deviations in state measurements from the baseline. Fig. 3 is a schematic of the nonlinear and linear controller used in conjunction. The baseline path in red is computed by the nonlinear solution while the green curve represents the true path. The state and control history with an asterisk, $*$, represents the baseline values while the state and control history without the asterisk is along the true path. At initial time, t_0, the control output is $\mathbf{u}_0$; also $\mathbf{u}_0 = \mathbf{u}_0^*$. Subsequently, the linear controller identifies corrective maneuvers, $\delta\mathbf{u}_k$, at time t_k. The net control maneuver ($\mathbf{u}_k$) delivered to the chaser is the sum of control outputs from the nonlinear ($\mathbf{u}_k^*$) and the linear controller ($\delta\mathbf{u}_k$), i.e., $\mathbf{u}_k = \mathbf{u}_k^* + \delta\mathbf{u}_k$. The frequency of the control outputs are consistent in the nonlinear and linear controllers. A summary of the blended linear and nonlinear controllers for proximity operations, along with vision based state estimation is presented in Fig. 4.

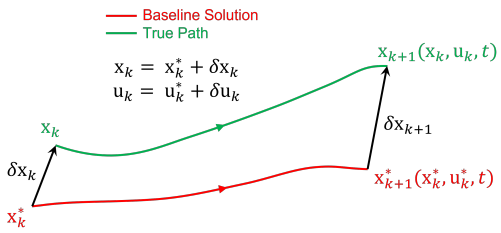

Fig. 3. Nonlinear control delivers a baseline/reference solution while linear controller compensates for any deviations from the baseline.

1) System Dynamics: A linear controller is employed to rapidly deliver control maneuvers to compensate for any deviations measured from the baseline path, i.e., $\delta\mathbf{x}_k$. The uncertainties in state measurements are small, and hence, linear dynamics near the baseline path is sufficient to predict an appropriate control output. Based on the variational equations of motion computed near the reference path (one computed in section III), the linear dynamics are governed by

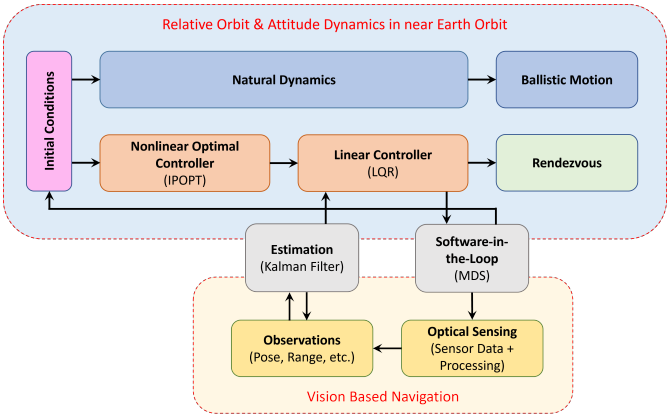

Fig. 4. Proximity operations: Control and estimation of satellites states.

$$\delta\mathbf{x}_{k+1} = \mathbf{A}_k\delta\mathbf{x}_k + \mathbf{B}_k\delta\mathbf{u}_k \tag{30}$$

where $\mathbf{A}_k$ is the 23×23 state transition matrix, and $\mathbf{B}_k$ is a 23×6 matrix that corresponds to the partials of state vector at final time, $\mathbf{x}_{k+1}$, to a control vector $\delta\mathbf{u}_k$, evaluated along the baseline path. The motion of the target and the approach site are independent from the motion of the chaser, therefore, a number of partials within the matrix $\mathbf{A}_k$ are zeros, Further, it is assumed that only the chaser satellite is controllable, hence, the control inputs do not affect the motion of the target body or the approach site; consequently, a number of partials within $\mathbf{B}_k$ are zeros. The sparse matrices $\mathbf{A}_k$ and $\mathbf{B}_k$ are computed numerically through central differencing technique.

2) Linear Quadratic Regulator (LQR): Control outputs are delivered at discrete intervals using a discrete LQR controller. Once the system is linearized along the baseline solution, a feedback controller is formulated that minimizes the cost functional, $\tilde{J}$, such that

$$\tilde{J} = \delta\mathbf{x}_N^{\mathrm{T}}\tilde{\mathbf{P}}_N\delta\mathbf{x}_N + \sum_{k=0}^{N-1}\delta\mathbf{x}_k^{\mathrm{T}}\tilde{\mathbf{Q}}_k\delta\mathbf{x}_k + \delta\mathbf{u}_k^{\mathrm{T}}\tilde{\mathbf{R}}_k\delta\mathbf{u}_k \tag{31}$$

and penalizes on any deviations in state from the baseline path, as well as on the size of control. The solution to this LQR problem is given by,[12, 13]

$$\delta\mathbf{u}_k = -\tilde{\mathbf{K}}_k\delta\mathbf{x}_k \tag{32}$$

where $\tilde{\mathbf{K}}_k$ is the time-dependent gain matrix that satisfies

$$\tilde{\mathbf{K}}_k = (\tilde{\mathbf{R}}_k + \mathbf{B}_k^{\mathrm{T}}\tilde{\mathbf{P}}_{k+1}\mathbf{B}_k)^{-1}\mathbf{B}_k^{\mathrm{T}}\tilde{\mathbf{P}}_{k+1}\mathbf{A}_k \tag{33}$$

and $\tilde{\mathbf{P}}_k$ satisfies the discrete algebraic Riccati equation,

$$\tilde{\mathbf{P}}_k = \tilde{\mathbf{Q}}_k + \mathbf{A}_k^{\mathrm{T}}\tilde{\mathbf{P}}_{k+1}\mathbf{A}_k - \mathbf{A}_k^{\mathrm{T}}\tilde{\mathbf{P}}_{k+1}\mathbf{B}_k\tilde{\mathbf{K}}_k \tag{34}$$

for $k = 0, \ldots, N-1$. Each of $\tilde{\mathbf{Q}}_k$ and $\tilde{\mathbf{R}}_k$ are positive definite weighting matrices or penalty matrices. The quantity N is the total number of discrete segments of the approach path considered for proximity operations.

Note that the intervals between state estimation using Kalman filter is different from that of the delivery of the control outputs. Kalman filter is applied to process the readings from the optical sensors, subsequently refines measurements at a significantly higher frequency than the algorithm that delivers control outputs for the chaser satellite. A sufficient time span is required between two successive control outputs for estimating the spacecraft's position, velocity and orientation states with reasonable precision. A symbolic representation of the observations, estimation and control timeline is presented in Fig. 5. High frequency pose observations are indicated by magenta dots. Larger red dots correspond to intervals of control maneuverand the red curve serves as the baseline for the rendezvous operations. Green curve in Fig. 5 is equivalent to the true path that the satellite traverses once the uncertainties in state measurements are incorporated.A gray dotted curve is the continuously estimated path once the observed data is processed through the Kalman filter. A solid blue curve reflects the ballistic motion if no control outputs are delivered.

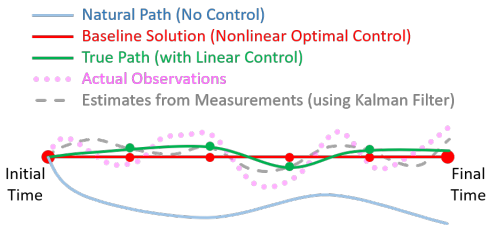

Fig. 5. Time history of natural path, optimal path for rendezvous and true path. Red and green dots correspond to intervals of control outputs, while magenta dots corresponds to the intervals for pose/range/LOS observations.

V. Perception

Vision is chosen for implementation of the navigation part of the chaser due to a significant portion of the information being present in the visual spectrum. Using visual data, certain features of the target body are derived, including relative pose of the body and distance measurements. Using the vision sensor data with modern deep learning and computer vision techniques offers unprecedented robustness for different On-Orbit Servicing scenarios requiring proximity operations. The main algorithms developed for the navigation part include, Region of Interest (ROI) extraction (Fig. 6), pose estimation, from which line-of-sight and range may also be derived. In the initial phases of the development, synthetic data is utilized to train and test the vision-based navigation algorithms in real-time and in a multitude of different scenarios. The environmental variables such as lighting conditions and distance are varied to test the robustness of the navigation solution.

VI. Results

A. Controller characteristics

The final approach phase for the satellites are considered in this investigation where the trajectory and the orientation of both the chaser and target bodies are relevant. The effectiveness of the controller is validated with a complex rendezvous scenario involving a non-cooperative and tumbling target. The

Fig. 6. VBN: Region of Interest (ROI) extraction using Deep Learning.[14]

approach site is aligned with the face of the tumbling target satellite, in a 7000 km orbit with $r_{collision} = 1$m. The position history for such complex scenario is demonstrated in Fig. 7 while the rendezvous path and the control history are delivered in Fig. 8. Further, experiments with synthetic pose with high errors (3σ: 15 cm in x, y, z and 0.0015 in each ϵ_i) delivered at 2 seconds interval, including some delayed and missed poses are tested. The chaser traverses along the states estimated from prior observations and with the most recent uncertainty levels, in the neighborhood of the reference path. Such effects are evident in Fig. 7. Poor observations increase uncertainties in state estimation increasing any deviations from the baseline path; consequently, drives the control costs higher.

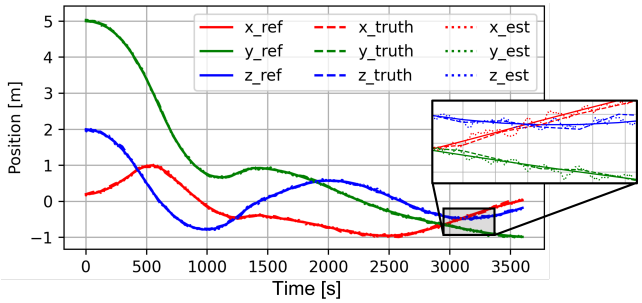

Fig. 7. Position state history (non-cooperative and tumbling target)

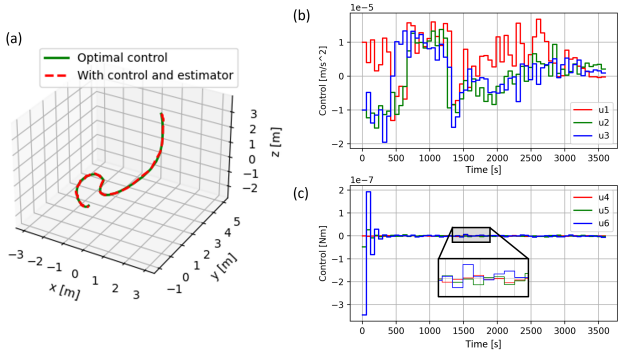

Fig. 8. Control for non-cooperative and tumbling target. (a) Trajectory in 3D space, (b) Acceleration control history, and (c) Torque control history

B. Software-in-the-loop integration

The MDS tool from Blackswan Space[14] is used to perform validation of the GNC algorithms. MDS allows to create a multitude of different OOS scenarios with target and chaser objects and test the performance of GNC algorithms used for proximity operations in real-time closed loop simulations

through MDS API. A visual representation of a sample rendezvous scenario is presented in Fig. 9 that validates software-in-the-loop architecture of the controller with the MDS toolkit. The target satellite (modelled as 8U CubeSat) is in a circular orbit of radius 7000 km around the Earth. The chaser at its initial state is 0.001° in True Anomaly (TA) behind the target, and 2 m in higher altitude; approximately corresponding to 12.2 m of separation. The rendezvous is achieved within 180 seconds during which the chaser arrives at the approach site 0.6 m behind the target. Consequently, the radius for the collision avoidance sphere, $r_{collision}$, is set to 0.6 m for the optimal control problem. Compatible with CubeSats, a maximum of 25 mN thrust level is considered. The MDS tool simulates an orbital environment and the cameras on the chaser extracts pose information. Stochastic uncertainties are present in the extracted target pose due to several factors including varying lighting conditions and from the algorithm that detects semantic features on the target body. Observations are filtered using the Kalman filter as described. Based on the state feedback received after filtering the pose data, maneuvers are delivered to compensate for any deviation from the reference path. Fig. 10 offers the evolution of position states along each coordinate axis during the rendezvous operation, for each of the reference path, true path and the estimate. The net control history in terms of linear acceleration and the control torque are given in Fig. 11. Control inputs are varied discretely at an interval of 3 seconds.

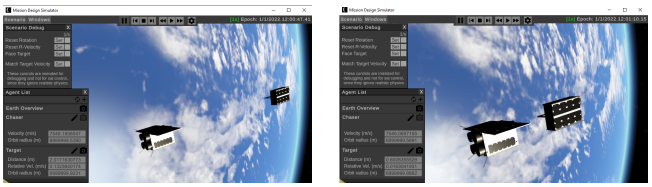

(a) Chaser approach (b) Approach site reached

Fig. 9. Proximity operations

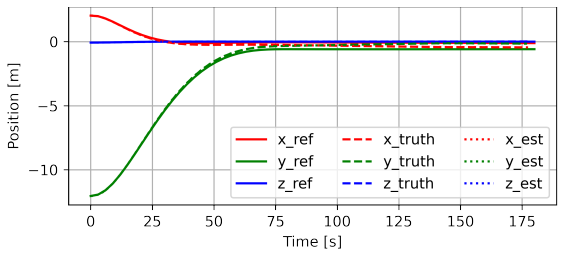

Fig. 10. Position state history

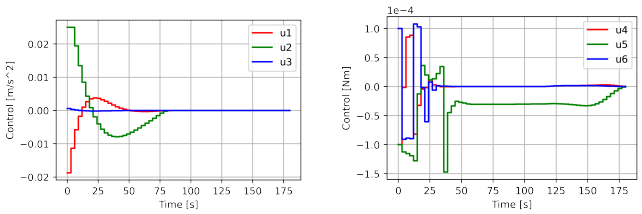

(a) Linear acceleration control (b) Torque control

Fig. 11. Control history

VII. Concluding Remarks

A harmonious blend of nonlinear optimal control algorithm with a linear state feedback control algorithm is exploited for their benefits, and is demonstrated for a complex rendezvous operation. An optimal controller evaluates the nonlinear model for the coupled attitude and orbit dynamics to deliver a reference solution. A linear state feedback controller offers the advantage of delivering maneuvers in real time by compensating any deviations from the predicted reference path. An application to vision-based navigation system for proximity operations with pose estimation is validated. Feasibility of such GNC algorithm will eventually be validated in a hardware-in-the-loop setup.

Acknowledgment

This work is supported by the Luxembourg National Research Fund INTER20/EUROSTARS/15254521. This project, E115088 - VBN, has received funding from the Eurostars-2 Joint Programme with cofunding from the European Union's Horizon 2020 research and innovation programme.

References

[1] A. C. Boley and M. Byers, "Satellite mega-constellations create risks in low earth orbit, the atmosphere and on earth," *Scientific Reports*, vol. 11, no. 1, pp. 1–8, 2021.

[2] W. Clohessy and R. Wiltshire, "Terminal guidance system for satellite rendezvous," *Journal of the Aerospace Sciences*, vol. 27, no. 9, pp. 653–658, 1960.

[3] D. Jezewski and J. Donaldson, "An analytic approach to optimal rendezvous using clohessy-wiltshire equations," *Journal of the Astronautical Sciences*, vol. 27, pp. 293–310, 1979.

[4] P. Palmer, "Optimal relocation of satellites flying in near-circular-orbit formations," *Journal of Guidance, Control, and Dynamics*, vol. 29, no. 3, pp. 519–526, 2006.

[5] J. E. Prussing, "Optimal two-and three-impulse fixed-time rendezvous in the vicinity of a circular orbit," *AIAA Journal*, vol. 8, no. 7, pp. 1221–1228, 1970.

[6] P. Singla, K. Subbarao, and J. L. Junkins, "Adaptive output feedback control for spacecraft rendezvous and docking under measurement uncertainty," *Journal of guidance, control, and dynamics*, vol. 29, no. 4, pp. 892–902, 2006.

[7] S. Vaddi, K. T. Alfriend, S. Vadali, and P. Sengupta, "Formation establishment and reconfiguration using impulsive control," *Journal of Guidance, Control, and Dynamics*, vol. 28, no. 2, pp. 262–268, 2005.

[8] M. Pagone, M. Boggio, C. Novara, and S. Vidano, "A Pontryagin-based NMPC approach for autonomous rendez-vous proximity operations," in *2021 IEEE Aerospace Conference (50100)*, pp. 1–9, IEEE, 2021.

[9] J. A. E. Andersson, J. Gillis, G. Horn, J. B. Rawlings, and M. Diehl, "CasADi – A software framework for nonlinear optimization and optimal control," *Mathematical Programming Computation*, vol. 11, no. 1, pp. 1–36, 2019.

[10] O. Montenbruck, E. Gill, and F. Lutze, "Satellite orbits: models, methods, and applications," *Appl. Mech. Rev.*, vol. 55, no. 2, pp. B27–B28, 2002.

[11] V. Muralidharan, A. Weiss, and U. V. Kalabic, "Control strategy for long-term station-keeping on near-rectilinear halo orbits," in *30th AIAA/AAS Space Flight Mechanics Meeting, Orlando, FL, USA*, January 2020.

[12] R. F. Stengel, *Optimal Control and Estimation*. Mineola, NY: Dover, 2nd ed., 1994.

[13] V. Muralidharan, A. Weiss, and U. V. Kalabic, "Tracking neighboring quasi-satellite orbits around phobos," in *World Congress of the International Federation of Automatic Control (IFAC)*, p. 14906–14911, Elsevier, 2020.

[14] "Mission Design Simulator - Blackswan Space," January 2022. Accessed on: March 23, 2022. [Online]. Available: https://www.blackswan.ltd/mission-design-simulator/.